
Article:
Zhang, Wei, Cziegler, Istvan orcid.org/0000-0003-1040-8918, Bobkov, V et al. (8 more authors) (2019) Blob distortion by radio-frequency induced sheared flow. Nuclear Fusion. 074001. ISSN: 1741-4326

https://doi.org/10.1088/1741-4326/ab1f1a

Blob distortion by radio-frequency induced sheared flow

W. Zhang[1,a)], I. Cziegler[2], V. Bobkov[1], G. D. Conway[1], G. Fuchert[3], M. Griener[1], O. Kardaun[1], P. Manz[1], J.-M. Noterdaeme[1,4], E. Seliunin[5], E. Wolfrum[1], the ASDEX Upgrade Team[1]

[1]*Max-Planck-Institut für Plasmaphysik, Garching, Germany*
[2]*University or York, York, United Kingdom*
[3]*Max-Planck-Institut für Plasmaphysik, Greifswald, Germany*
[4]*Applied Physics Department, University of Ghent, Ghent, Belgium*
[5]*Instituto de Plasmas e Fusão Nuclear, IST, Universidade de Lisboa, Lisboa, Portugal*

a) Corresponding author: wei.zhang@ipp.mpg.de

Abstract

Blob transport properties in the plasma edge in the presence and absence of radio-frequency (RF) convective cells are compared. For the first time, the interactions between RF convective cells and intermittent plasma blobs in the scrape-off layer (SOL) are observed with gas puff imaging in the ASDEX Upgrade tokamak. It is found that the RF convective cells induce a sheared flow in the far SOL, which is able to stretch, distort and even split the blobs poloidally. The observed phenomena indicate that an externally generated sheared flow in the SOL can be considered as a method to modify blob transport in a favorable way.

Plasma heating with waves in the Ion Cyclotron Range of Frequencies (ICRF) is a standard heating method in magnetically controlled fusion plasmas. It uses the fast wave to transport the wave energy from the antenna to the plasma center. However, the slow wave with a large electric field parallel to the background magnetic field is generated parasitically. It is considered as the source of nonlinear radio-frequency (RF) sheath rectifications [1-3] by accelerating the more mobile electrons to the wall and enhancing the sheath potential nonlinearly. The induced inhomogeneous sheath potential drives localized convective $E \times B$ flows (i.e. RF convective cells) in the scrape-off layer (SOL) [4-7], which influence the density in front of the antenna. These changes will in turn modify the RF near fields and RF sheath formation [8].

Previously, interest has been focused on understanding the formation of RF convective cells and their influence on the SOL density in steady state [9, 10] - on the time scale of seconds or sub-seconds. RF convective cells can however also influence the SOL density on a much smaller time scale (microseconds) by influencing the transport of blobs or filaments [11] and in turn affect the cross-field transport of particles and energies [12] as well as the power load on the first wall and divertor [13]. It is thus very important to understand the interaction between blobs and RF convective cells. In this letter, we present the first and direct experimental measurements of blob stretching/distortion and splitting by RF convective cells.

The experiments were carried out in deuterium low-confinement mode (L-mode) discharges at the ASDEX Upgrade tokamak [14] (R=1.65 m, a≈0.5 m) with the following plasma parameters: toroidal magnetic field B_T = -2.5 T, plasma current I_p = 0.8 MA, safety factor q_{95} = 5.0, edge line integrated density $n_e = \ 3.0\mathrm{e}19\ m^{-3}$. As for the auxiliary heating, either Ion Cyclotron Resonance Heating (ICRH) or Electron Cyclotron Resonance Heating (ECRH) of 600 kW is used. ICRH used a standard D (H) minority scenario with RF frequency of f_0 = 36.5 MHz and a strap phasing (+90^o) generating large convective cells. Two heating scenarios were set in the discharges: the first scenario is with ECRH while the second scenario is with ICRH (see Fig. 1). This is to generate one scenario without RF convective cells and another scenario with RF induced convective cells. In our studied discharge #34676, ICRH is switched off during the time period of [2.0, 3.0s] and switched on during the next time period of [3.0, 4.0s]. With these settings, the effect of RF convective cells on blob transport can be characterized by comparing the blob behaviors in the two scenarios. Other plasma parameters, including the total heating power, are kept constant during this discharge.

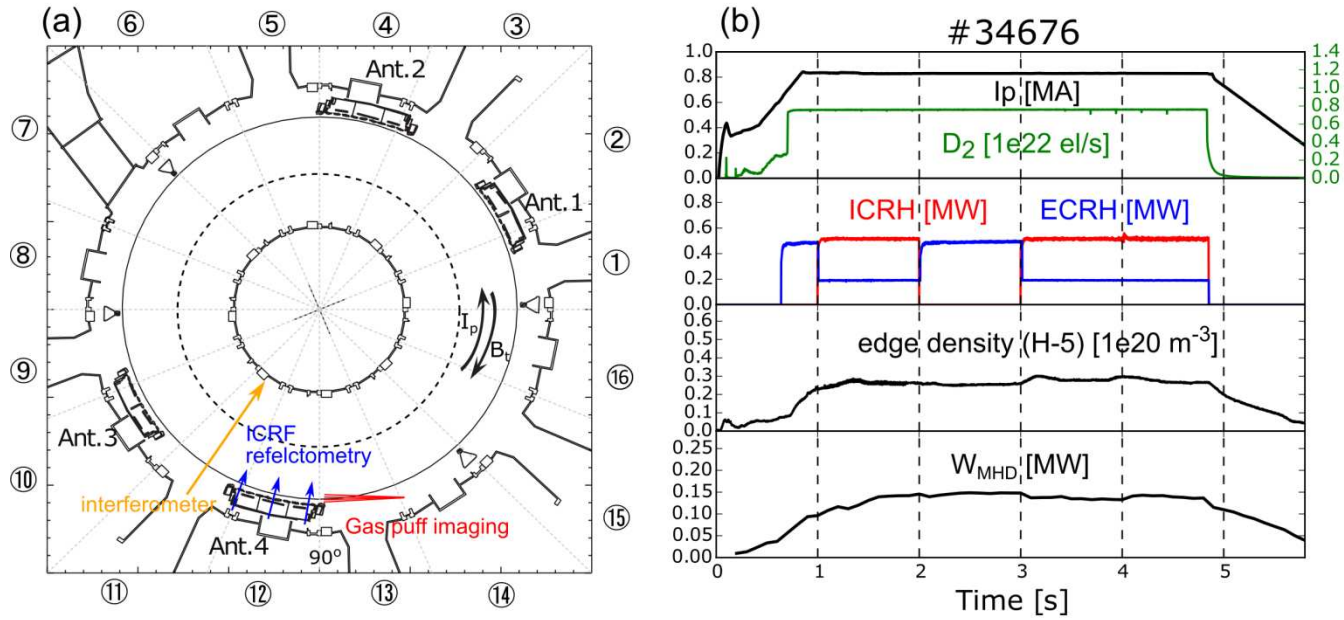

Figure 1. (1) Top view of ASDEX Upgrade and the locations of some key diagnostics such as GPI, reflectometry and interferometer near the ICRF antenna. (2) Plasma parameters, including the plasma current, gas fueling rate, auxiliary heating power, integrated edge line density and stored plasma energy of discharge #34676.

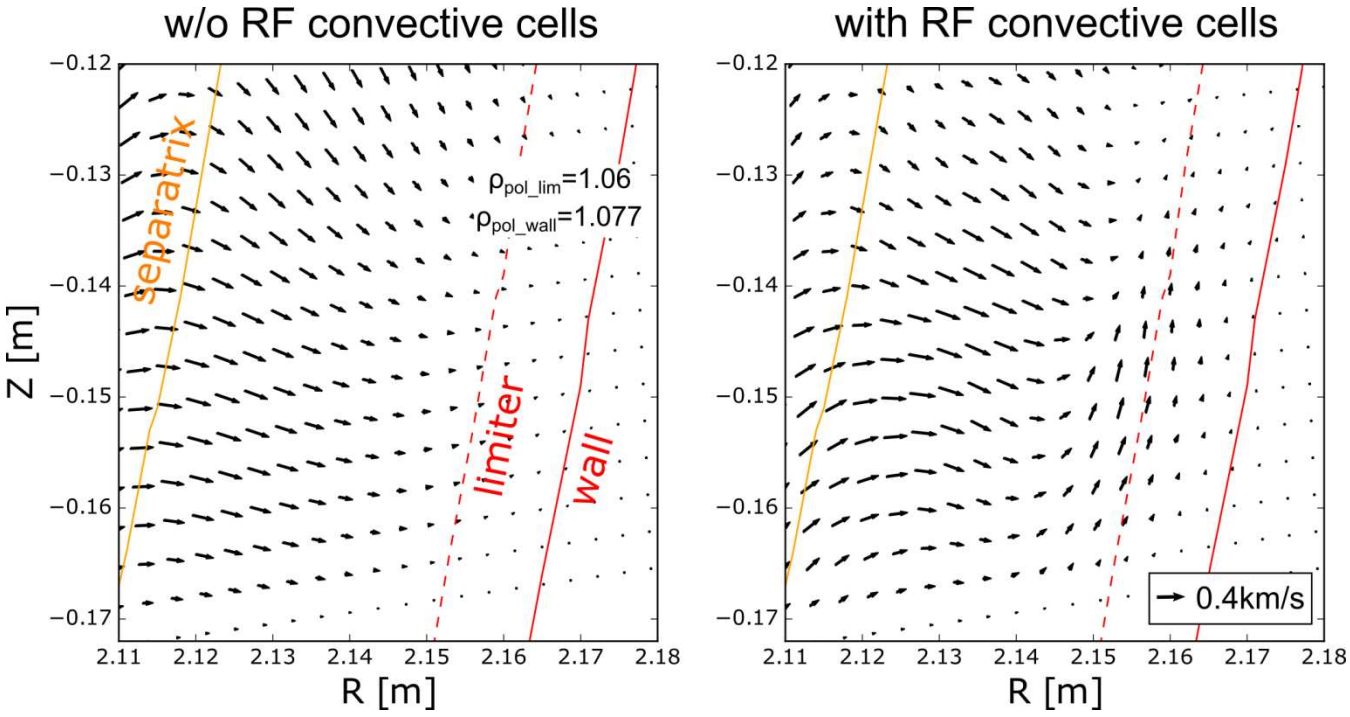

Figure 2. Averaged plasma velocity for scenarios without and with RF convective cells. The averaged time periods are [2.0, 2.01s] and [3.0, 3.01s], respectively.

Because the generated RF convective cells are poloidally localized in front of the powered antenna and toroidally elongated along flux tubes, the gas puff imaging (GPI) diagnostic [15] close to one of the powered antennas was used to measure the dynamics of the blob transport. The field of view of the GPI covers the plasma edge and the SOL, with a viewing area of ~ 16 × 8 cm^2 (poloidal × radial) and a time resolution of 5 μs. The corresponding pixels of the viewing area are 128 × 64 (poloidal × radial). The center of the viewing area is at 2.125 m and -0.148 m in the radial and poloidal directions, respectively.

The averaged 2D plasma velocity for scenarios without and with RF convective cells in the SOL are calculated with the Horn–Schunck optical flow method [16] based on the GPI data. The Horn-Schunck method is a classical optical flow estimation algorithm. It assumes smoothness in the flow over the whole image. Thus, it tries to minimize distortions in flow and prefers solutions which show more smoothness. An iteration number of 1000 and a regularization constant of 5 are set in the applied Horn-Schunck algorithm. The calculated flow velocity is averaged over a period time of [2.0, 2.01s] and [3.0, 3.01s] for the cases without and with RF convective cells, respectively. The results (Fig. 2, right) clearly show that a sheared plasma flow, being part of the RF convective cells, is developed in the far SOL for scenarios with RF convective cells. In typical L-mode plasmas in AUG, the convective cells measured with the Retarding Field Analyzer (RFA) usually extend radially by 1-2cm from the antenna leading edge into the SOL [17, 18], which is consistent with the sheared flow measured by GPI. Because the helium gas cloud used for the GPI diagnostic has a limited spatial spreading, the $E \times B$ velocity in the periphery of this gas cloud where the signal is low tends to be underestimated, for instance in regions with R > 2.15 m and Z > -0.142 m or Z < -0.165 m.

The velocity of sheared flow generated by the RF convective cells and its derivative (dv/dr) are usually of the order of km/s and 10^5 s^{-1}, respectively. They are of the same level as those self-generated by the plasma in the pedestal region. The latter play a critical role in forming a transport barrier in the pedestal and improving plasma confinement in the H-mode. Since the sheared flow generated by the RF convective cells is located in the far SOL (outside the confined plasma region), it is unlikely that it will have an influence on the confinement. However, it is expected that this sheared flow will have an influence on blob transport in the SOL.

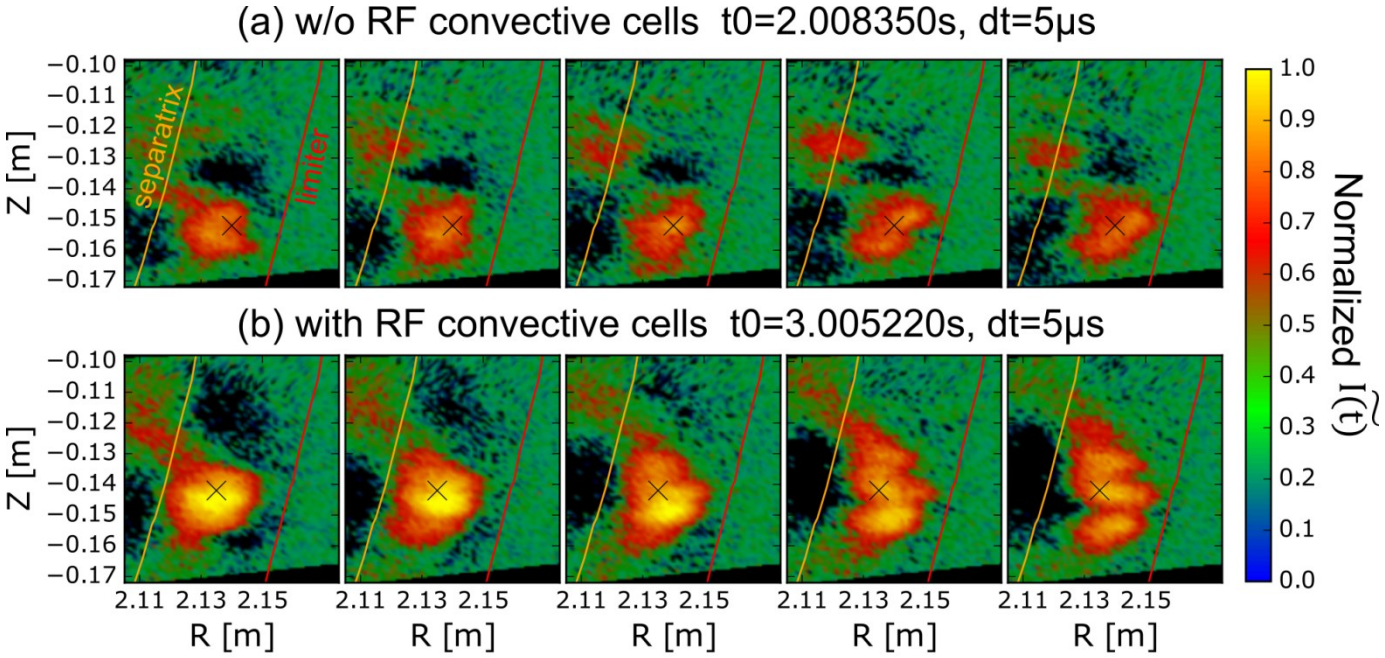

Figure 3. Dynamical evolution of blobs for scenarios without and with RF convective cells. The separatrix is denoted with the orange line and the antenna limiter is denoted with the red line. The regions of red / yellow color represent density blobs. The cross marks a fixed reference location to visualize blob propagation. The intensity of blobs is normalized to its maximum value.

To understand how the RF convective cells influence the blob transport, the blob dynamical evolutions for scenarios without and with RF convective cells are compared. In the analysis of GPI, the intensity of a blob is calculated by $\widetilde{I(t)} = I(t) - \sum_{t-20dt}^{t+20dt} I(t)/41$, in which dt = 5μs is the time difference between two adjacent GPI frames. An example is shown in Fig. 3. It can be seen that for scenarios without RF convective cells, the blob transports radially outward with just a gradual change of shape; for scenarios with RF convective cells, the blob is firstly poloidally stretched and then it is torn apart into smaller pieces as it moves further outward. Whether the blobs are only stretched or torn apart into smaller pieces depend on the magnitude of the $E \times B$ flow shear [19]. Similar behaviors of blob stretching and/or splitting by the sheared flow has been observed in the pedestal during plasma biasing [20]. For the SOL this is in particular beneficial because, as the blobs become stretched poloidally, the interaction area between the blob and the first wall is increased. This can lead to a reduction of radial transient heat load on the first wall. However, since the total volume of the blobs remains almost the same, it is expected that the total heat load on the divertor plates can hardly be changed.

(a) number of blobs

#34676, # of blobs for single ejection			
	#1	#2	#3
RF off	276	71	8
RF on	152	54	15

#34678, # of blobs for single ejection			
	#1	#2	#3
RF off	215	59	6
RF on	144	48	6

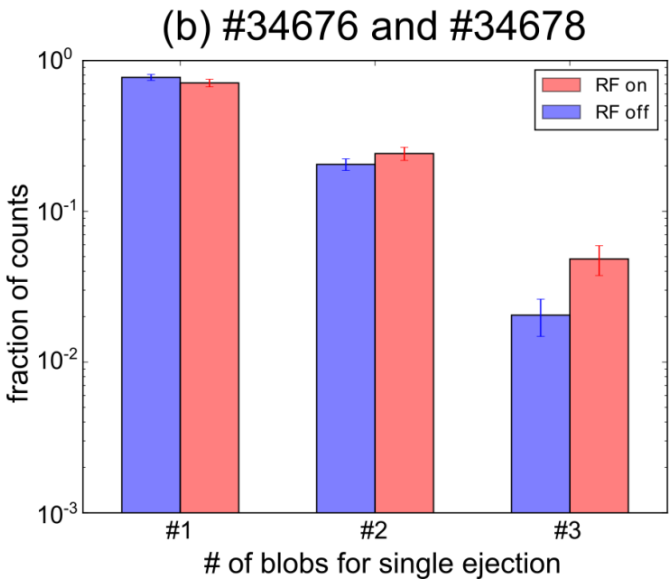

Figure 4. (a) Number of peaks in the poloidal direction after propagating into the far SOL for a single intermittent ejection event. Data of discharges #34676 and #34678 are used, in which #34678 is a repetition of #34676. The time of consideration is [2.0, 2.158s] and [2.8575, 3.0s] for the RF off case, [3.03, 3.138s] and [3.8575, 4.0s] for the RF on case. A shorter time period [3.03, 3.138s] (in comparison with [2.0, 2.158s]) is used for the RF on case considering the quality of the measured signals. #1 means no blob splitting, #2 means splitting into two pieces and #3 means splitting into three pieces. (b) Fraction of counts of blob splitting by combining the data of #34676 and #34678.

Moreover, blobs have also been observed to break up as they travel into the far SOL, as demonstrated in Fig. 4. Thus, the statistics of blob splitting is investigated. A trigger was set up in the middle SOL region, based on a local intermittency measure [21], to identify blobs. The poloidal structure was subsequently extracted by examining the poloidal brightness distribution along the flux surface to which the blob center propagated in 10us. Fig. 3(b) is the resulting statistics, comparing the number of peaks appearing poloidally at the lagged time to those at the trigger location in space-time with and without RF. The counting convention takes into account multiple peaks already existing at the trigger time. The histograms were built using 419 blobs with RF convective cells, and 635 blobs without, based on two similar discharges (#34676 and #34678) and the plotted errors represent the standard error, estimated as the square root of counts in each bin based on a no-memory time statistic of blob detection. Here only the percentage of each splitting is important. While the histogram with RF shows a larger number of broken blobs, the difference from no-RF appears to be within error bars for the first two columns. In the case of filaments breaking into 3 blobs, we see no overlap of the error bars and a seemingly intensified blob splitting by RF convective cells.

To improve the assessment whether the RF convective cells cause more blob splitting, we sum the events of blob splitting (i.e. #2 and #3 in Fig. 4(a)) together and use the standard normal approximation

to the difference of two binomial distributions to estimate the probability of equivalence of the "RF on" and "RF off" cases. The pertinent calculation yields the z-scores, calculated with $z = (\hat{P}_2 - \hat{P}_1)/SD(\hat{P}_2 - \hat{P}_1)$, are 2.34 and 1.0 for #34676 and #34678, respectively. The combined z-score is equal to $(2.34 + 1.0)/\sqrt{2} \approx 2.36$, corresponding to a right-tail probability of $1 - \Phi(z) = 1\%$. According to Fisher's fiducial argument [22], the likelihood that the "RF on" case is equal to the "RF off" case, just outside a 98% two-sided confidence interval for $\hat{P}_2 - \hat{P}_1$, is rather tiny, about 2.5%. This means that there is statistical evidence from these experiments that the RF convective cells lead to some intensified blob splitting. In fact, the estimated odds ratios, $\hat{P}_2(1 - \hat{P}_1)/\hat{P}_1(1 - \hat{P}_2)$, for blob splitting are (69×276)/(152×79)=1.6 (#34676) and (54×215)/(144×65)=1.25 (#34678), with corresponding $\pm$2STD interval estimates [23] of (1.43, 1.75) and (1.1, 1.4), respectively.

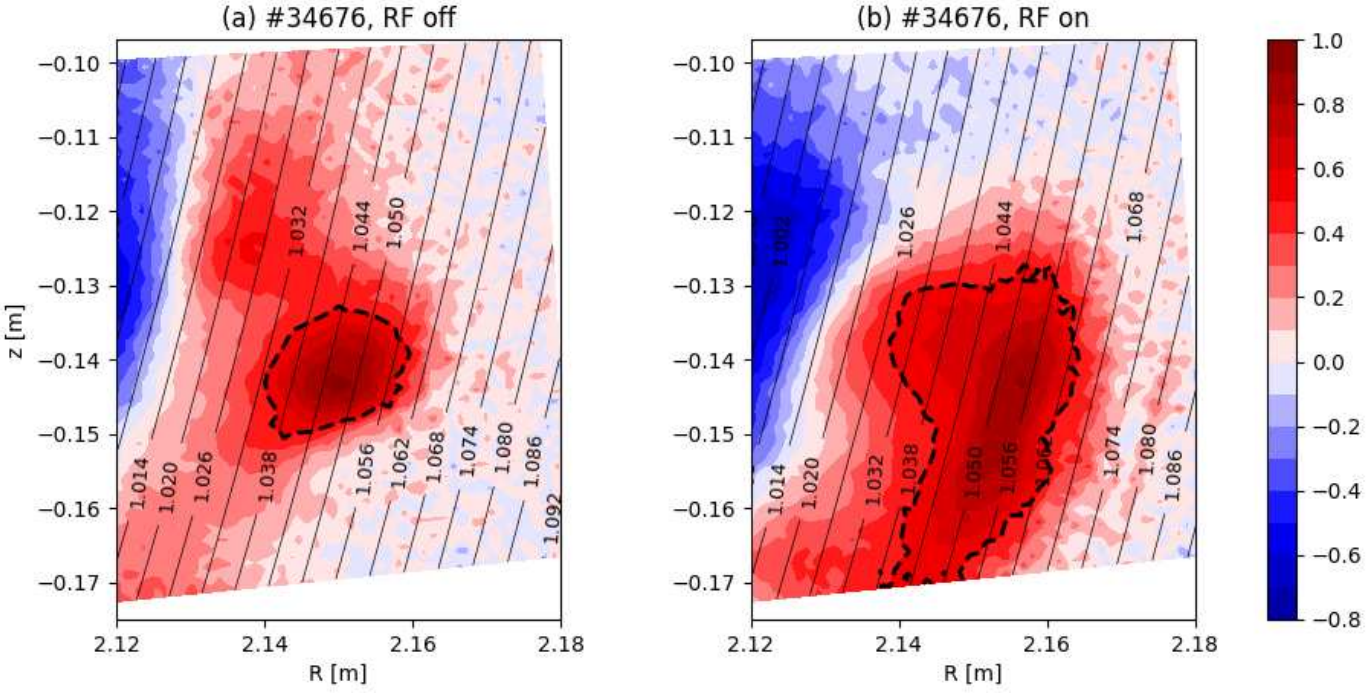

Figure 5. Comparisons of correlation values for scenarios (a) without and (b) with RF convective cells. The time intervals used in the analysis are [2.06, 2.061s] and [3.032, 3.033s], respectively. The poloidal black lines indicate the positions of ρ_{pol}.

For turbulence suppression, tilting and stretching are sufficient while breaking apart the structure is not necessary [24]. Due to the tilting, fluctuation amplitude is transferred from the fluctuations to the mean flow, leading to a reduction of the fluctuation amplitude [25, 26]. Due to the stretching, the structure is compressed in the direction perpendicular to it, leading to a higher dissipation [24]. To examine the effect of the sheared flow in the convective cells on the cross-sectional shape of the blobs,

we used GPI to record fluctuations in an area magnetically mapped to the front face of the antenna. Fig. 5 compares results of the measurement with and without an active antenna, based on a cross-correlation over 1 ms of signal with a lag of zero, using a reference signal at $\rho_{\mathrm{pol}} \approx 1.05$. Here $\rho_{\mathrm{pol}} = \sqrt{\psi_{\mathrm{N}}}$, in which ψ_{N} is the normalized toroidal flux, such that it is 0 on the magnetic axis and 1 at the separatrix. Since the fluctuation power in the far SOL is dominated by blob filaments, the correlation pattern is a measure of an average blob shape, i.e. filament cross-section. While the contour of the highly (> 0.5) correlated region in Fig. 5(a) shows an approximately circular structure, the one in Fig. 5(b) is strongly elongated in the poloidal direction. This is direct evidence of blob distortion and stretching in the convective cell of a powered ICRF antenna. The stretching of the structure is directly related to enhanced dissipation as explained above.

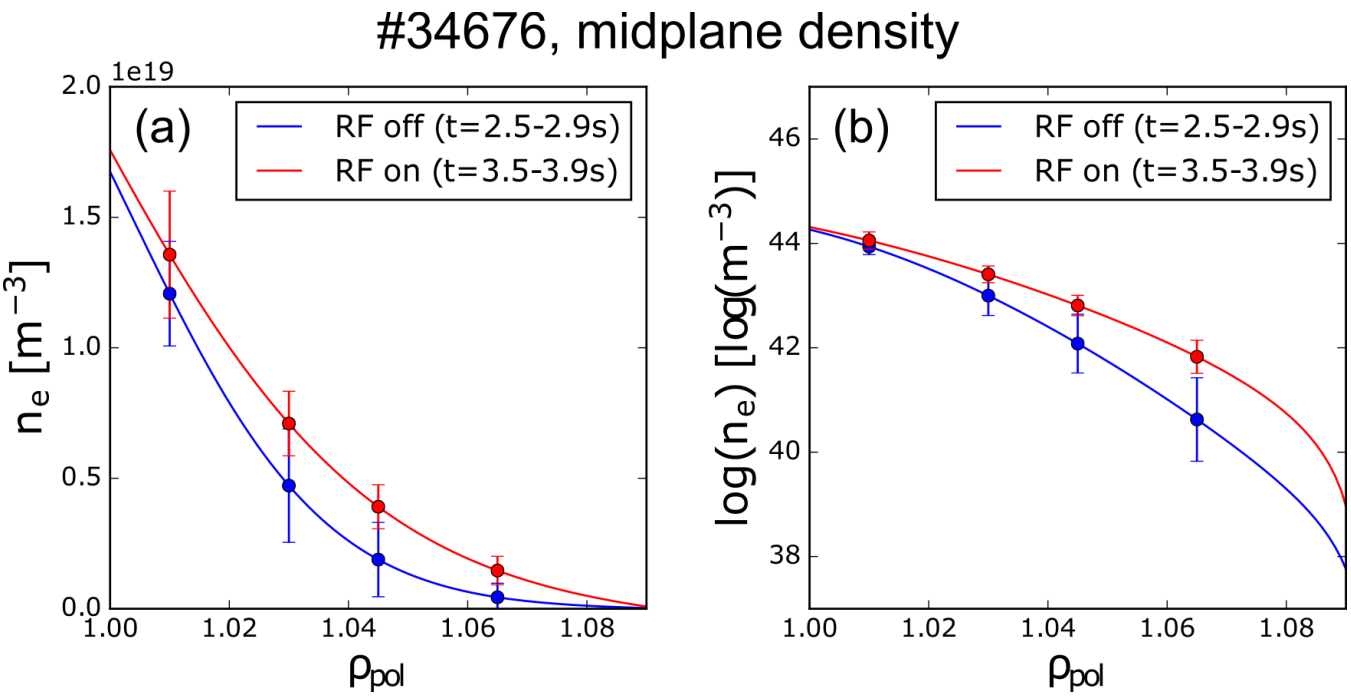

Figure 6. (a) Midplane density for scenarios without and with RF convective cells. The averaged time intervals are [2.5, 2.9s] and [3.5, 3.9s], respectively. $\rho_{pol} = 1.0$ is the position of separatrix. (b) Same density profiles in log scale.

The induced sheared flow not only distorts and splits blobs in the far SOL, but can also have the capability of blob stopping due to the collapse of the radial velocity of the blobs within the shear layer [27]. The interpretation is as follows: as more blobs are stopped by the sheared flow in the far SOL, the midplane density in the SOL is increased while the separtrix density remains the same, as shown in Fig. 6. In addition, it is hypothesized that blob stopping can be beneficial for stabilizing divertor plasma detachment by increasing the upstream and downstream density in the SOL. More work is ongoing to understand this.

Enhanced blob activity as observed during detachment [28, 29] will not only spread the power across the divertor region, but also enhance the heat flux to the first wall. The first wall is however not designed for enhanced heat fluxes. As shown here, externally generated sheared flows acting like a transport barrier can lead to stopping of the blobs. If this transport barrier is designed to be at the outer border of the divertor region, heat and particle transport is spread by the blobs across the divertor region and the blobs reach only the outer divertor region, a region designed to withstand enhanced heat flux. Furthermore, the enhanced parallel particle flux due the transport barrier can possibly facilitate detachment, as the overall density is the divertor increases. More importantly, the first wall would be still protected by the transport barrier. More work on these aspects is ongoing.

In summary, the influence of externally generated RF convective cells on blob transport is observed and analyzed for the first time. It is shown that the RF convective cells generate sheared $E \times B$ plasma flow in the far scrape-off layer (SOL). This sheared flow is able to stretch, distort and even split blobs poloidally. In addition, it can cause blob stopping, which may facilitate divertor detachment. Thus, externally generating sheared flow in the SOL can be considered as a method to modify the blob transport in the SOL. It may also be considered as a potential way to control the heat fluxes to the first wall and divertor region through blob stopping in the sheared velocity region.

Acknowledgments: This work has been carried out within the framework of the EUROfusion Consortium and has received funding from the Euratom research and training programme 2014-2018 and 2019-2020 under grant agreement No 633053. The views and opinions expressed herein do not necessarily reflect those of the European Commission.

[1] Butler H. S. *et al* 1963 *Physics of Fluids* **6** 1346-55
[2] D'Ippolito D. A. *et al* 2006 *Physics of Plasmas* **13** 102508
[3] Bobkov V. *et al* 2017 *Plasma Phys. Control. Fusion* **59** 014022
[4] Becoulet M. *et al* 2002 *Physics of Plasmas* **9** 2619-32
[5] D'Ippolito D. A. *et al* 1993 *Physics of Fluids B-Plasma Physics* **5** 3603-17
[6] Hong R. *et al* 2017 *Plasma Physics and Controlled Fusion* **59** 105008
[7] Martin M. J. *et al* 2017 *Physical Review Letters* **119** 205002
[8] Zhang W. *et al* 2017 *Nuclear Fusion* **57** 116048
[9] Noterdaeme J. M. *et al* 1993 *Plasma Physics and Controlled Fusion* **35** 1481-511
[10] Myra J. R. *et al* 2006 *Nuclear Fusion* **46** S455-S68
[11] D'Ippolito D. A. *et al* 2005 *AIP Conference Proceedings* **787** 222-5
[12] Krasheninnikov S. I. *et al* 2008 *Journal of Plasma Physics* **74** 679-717
[13] Thornton A. J. *et al* 2015 *Plasma Physics and Controlled Fusion* **57** 115010
[14] Kallenbach A. *et al* 2017 *Nuclear Fusion* **57** 102015
[15] Fuchert G. *et al* 2014 *Plasma Physics and Controlled Fusion* **56** 125001

[16] Horn B. K. P. *et al* 1981 *Proceedings of the Society of Photo-Optical Instrumentation Engineers* **281** 319-31
[17] Colas L. *et al* 2013 *AIP Conference Proceedings* **1580** 259-62
[18] Zhang W. *et al* 2016 *Plasma Phys. Control. Fusion* **58** 095005
[19] Biglari H. *et al* 1990 *Physics of Fluids B-Plasma Physics* **2** 1-4
[20] Shesterikov I. *et al* 2013 *Physical Review Letters* **111** 055006
[21] Farge M. 1992 *Annual Review of Fluid Mechanics* **24** 395-457
[22] Fisher R. A. 1973 *Statistical Methods and Scientific Inference* New York Hafner Press
[23] Sachs L. 1984 *Applied Statistics: A Handbook of Techniques (Springer Series in Statistics)*
[24] Manz P. *et al* 2009 *Physical Review Letters* **103** 165004
[25] Manz P. *et al* 2012 *Physics of Plasmas* **19** 072311
[26] Cziegler I. *et al* 2017 *Physical Review Letters* **118** 105003
[27] Ghendrih P. *et al* 2009 *Journal of Nuclear Materials* **390-91** 425-7
[28] Carralero D. *et al* 2014 *Nuclear Fusion* **54** 123005
[29] Carralero D. *et al* 2015 *Physical Review Letters* **115** 215002